Appl Phys A (2012) 109:101–109
DOI 10.1007/s00339-012-7043-y

Applied Physics A
Materials Science & Processing

Simulation of impact of a hollow droplet on a flat surface

Arvind Kumar · Sai Gu · Spyros Kamnis

Received: 25 April 2012 / Accepted: 27 June 2012 / Published online: 14 July 2012

Abstract Despite many theoretical and experimental works dealing with the impact of dense continuous liquid droplets on a flat surface, the dynamics of the impact of hollow liquid droplets is not well addressed. In an effort to understand dynamics of the hollow droplet impingement, a numerical study for the impact of a hollow droplet on a flat surface is presented. The impingement model considers the transient flow dynamics during impact and spreading of the droplet using the volume of fluid surface tracking method (VOF) coupled with the momentum transport model within a one-domain continuum formulation. The model is used to simulate the hydrodynamic behaviour of the impact of glycerin hollow droplet. It is found that the impact and spreading of the hollow droplet on a flat surface is distinctly different from the conventional dense droplet and has some new hydrodynamic features. A phenomenon of formation of a central counter jet of the liquid is predicted. With the help of simulations the cause of this phenomenon is discussed. Comparison of the predicted length of the central counter jet and the velocity of the counter jet front shows good agreements with the experimental data. The influence of the droplet initial impact velocity and the hollow droplet shell thickness on the impact behaviour is highlighted.

Abbreviations

D_0 Initial droplet diameter, m
d Initial void diameter, m
F Volume of fluid function
$\vec{g}$ Acceleration due to gravity vector, m/s^2
Re Reynolds number ($\rho D_0 U_0/\mu$)
T Temperature, K
t Time, s
U_0 Initial droplet velocity, m/s
$\vec{u}$ Continuum velocity vector, m/s
We Weber number ($\rho D_0 U_0^2/\sigma$)

Greek symbols

μ Dynamic viscosity, kg·m^{-1}/s
ρ Density, kg/m^3
σ Droplet surface tension, N/m

Subscript

d Droplet
air Air
0 Initial

A. Kumar · S. Kamnis
School of Engineering Sciences, University of Southampton, Southampton SO17 1BJ, UK

S. Gu (✉)
School of Engineering, Cranfield University, Cranfield MK43 0AL, UK
e-mail: s.gu@cranfield.ac.uk

1 Introduction

The principle of droplet impingement on a solid surface is relevant to many engineering applications (e.g., thermal spray coating, spray forming, spray painting, spray cooling of hot surfaces, ink-jet printing, solder deposition on printed circuit boards, etc.). Significant effort is being devoted to the modelling and simulation of the droplet impact process [1–5]. These modelling efforts are well reviewed by Kamnis and Gu [2] and Chandra and Fauchais [4]. Modelling droplet impact on surfaces has improved the understanding of droplet deformation and adhesion with the surfaces, for example in the thermal spray coating process where molten droplet of melt powder particles are projected towards the substrates to form protective coating on them.

Validation of these models has substantiated their ability to successfully predict the droplet spreading behaviour after impact with the substrate [1, 2, 4] with the correct number of fingers surrounding a three-dimensional splat [3]. These theoretical studies of droplet impingement [1–4], however, assume that the droplet is continuous without any voids inside. The impact of a hollow droplet onto the substrate and its spreading behaviour can differ fundamentally from a dense continuous droplet. New possibilities for thermal spraying of functional coatings formed by deposition of hollow melt droplets are discussed in the work by Solonenko et al. [6, 7]. In this connection, the investigation of the impact of a hollow melt droplet onto a solid substrate is of scientific and applied importance. To the best of authors' knowledge, there is only one experimental study where visualisation of the collision of a hollow liquid droplet of glycerin with a flat surface is reported [8].

The hollow and porous particles of metals, alloys, oxides, and other ceramics may be obtained by plasma processing of various powder materials [6, 7]. The presence of voids in the feedstock powders also have a great influence on the particle in-flight behaviours in the thermal spray coating process such as, particle acceleration, melting, and oxidation because a hollow particle is also lighter than a dense one and this can affect the particle trajectory. Very recently, computational results for porous and hollow powder particles in-flight behaviour show that these particles are accelerated to higher velocity with higher surface temperatures than fully solid powders [9]. Air voids in the porous and hollow powder particles form from spray dried agglomerates [6, 7, 9, 10]. These porous powder particles during their in-flight motion in the thermal plasma jet form hollow liquid droplets prior to their impact with the surface [7, 8]. The limited studies reported in this field [6, 7, 11] show that coating using hollow melt droplets opens up new prospects for the application of porous and hollow powders for making thermal coatings with substantially improved characteristics (e.g., adhesion, controlled porosity in the coating, and coating structure). Controlling the coating porosity thermal insulation properties of the coatings can be enhanced [12], which will have potential applications in turbine blade, engine component coatings. Despite many theoretical and experimental works dealing with the dense continuous liquid droplets, the dynamics of the impingement of hollow droplet is not well addressed, and hence the current understanding of the behaviour of hollow particles in thermal spray is very limited. A clear understanding of the impact dynamics of hollow droplet on the surface of substrates is needed. The understanding of the hydrodynamic behaviour of the hollow droplet impact will be a starting step to systematically investigate the coating formed by hollow melt droplets.

The objective of this work is to investigate the impact and spreading behaviour of a hollow droplet onto a flat surface using numerical model and simulations. In the model transient flow dynamics during impact and spreading are considered with the help of the volume of fluid surface tracking method (VOF) coupled with droplet momentum transport within a one-domain continuum formulation. The features of hollow droplet impact, including a phenomenon of formation of a central counter jet of liquid, are discussed. The length of the central counter jet and the velocity of the counter jet front are compared with the experimental data. The droplet impact behaviour for different droplet impact velocities and hollow droplet shell thickness are also discussed.

2 Numerical simulations

We consider the problem corresponding to the benchmark experiment for the impact of a hollow droplet of glycerin [8]. The experiment was designed such that the influence of heat exchange and phase transitions is minimal, so that the main attention is concentrated on the hydrodynamic features of liquid spreading that is on the role of viscosity and surface tension of the liquid [8]. Accordingly, in the present model problem also we exclude heat transport and phase transitions and focussed on the hydrodynamic behaviour. The conditions were chosen similar to those in the experiment [8] such as, Reynolds numbers (Re), Weber numbers (We), and droplet shell thicknesses are typical of the conditions of plasma spray coating deposition. In addition, the conditions were selected to obey the relation $We/Re = 10$–100, which implies that the viscosity effects predominate over the surface tension during the spreading of the droplet [8]. Immediately prior to droplet-surface collision, the droplet consists of a liquid shell enclosing a gas (air) cavity. For this, a molten glycerin hollow spherical droplet with an outer diameter (D_0) 5.25 mm and void (of air) diameter (d) 4.389 mm is considered to impinge with a velocity (U_0) of 5.94 m/s onto a flat surface. We refer to these impact conditions as the baseline case. We have considered a two-dimensional axisymmetric formulation and Fig. 1 shows the schematic of the computational domain. The domain consists of 150,000 structured computational cells with a refined mesh near the surface. Table 1 shows the material properties data used for the current problem.

2.1 Governing transport equations

2.1.1 Free surface modelling

The VOF model is used to track the interface between the droplet and the air considering these two as immersible fluids by solving a single set of momentum equations. This method tracks the volume fraction of each of the fluids throughout the computational domain. Accordingly, the

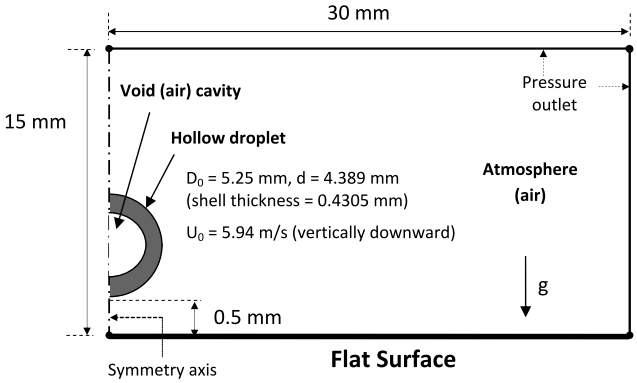

Fig. 1 Schematic diagram of the axisymmetric computational domain

Table 1 Material properties data

Impinging droplet material	Glycerin
Gas phase (the void and the droplet surrounding medium)	Air
Density of the droplet	1261 kg/m^3
Density (air)	1.225 kg/m^3
Droplet surface tension	0.0634 N/m
Droplet viscosity	0.142 kg·m^{-1}/s
Air viscosity	1.7894×10^{-5} kg·m^{-1}/s
Contact angle	140°
Surface tension coefficient	−0.00036 N·m^{-1}/K

governing equations are being solved in both air and molten droplet domains. The volume of fraction of fluid in a control volume (F) has a range from zero to unity; the cells having F values between zero and one ($0 < F < 1$) represent the air- molten droplet interface, $F = 0$ indicates that the cell contains only air, and $F = 1$ corresponds to a cell full of droplet material. The volume of fraction function F is advected using the continuum mixture velocity field $\vec{u}$ with the following transport equation:

$$\frac{\partial F}{\partial t} + \nabla \cdot \vec{u} F = 0 \tag{1}$$

The interface treatment between the droplet phase and air phase is accomplished via a geometric reconstruction scheme detailed in [13].

2.1.2 Fluid flow modelling

In the current model, a continuum formulation with a one-domain approach based on the classical mixture theory is adopted [2]. The volume-fraction-averaged continuum density in each control volume can be calculated according to the fraction of the droplet fluid (F).

$$\rho = F\rho_{\mathrm{d}} + (1 - F)\rho_{\mathrm{air}} \tag{2}$$

where the subscripts 'd' and 'air' are for the droplet and the air phase, respectively. The density of air is assumed to be constant in the current model. Other volume-fraction-averaged properties are also defined in a similar manner.

$$\mu = F\mu_{\mathrm{d}} + (1 - F)\mu_{\mathrm{air}} \tag{3}$$

The volume-fraction-averaged material properties are then used in the momentum transport equations. The momentum conservation equation is coupled with the VOF model. Assuming the flow to be Newtonian, incompressible, and laminar, the governing equations for mass and momentum conservation can be written as follows.

$$\textit{Continuity}: \quad \frac{\partial}{\partial t}(\rho) + \nabla \cdot (\rho \vec{u}) = 0 \tag{4}$$

$$\begin{aligned} \textit{Momentum}: \quad & \frac{\partial}{\partial t}(\rho \vec{u}) + \nabla \cdot (\rho \vec{u}\vec{u}) \\ & = -\nabla p + \nabla \cdot \left[\mu\left(\nabla \vec{u} + \nabla \vec{u}^T\right)\right] \\ & \quad + \rho \vec{g} + F_{\mathrm{vol}} \end{aligned} \tag{5}$$

The fluid surface tension force at the boundary between the droplet and the surrounding gas is included as a body force, F_{vol}, in the momentum conservation equation [2], its value appears as a source term on the right-hand-side of the momentum conservation equation (Eq. (5)). This term is calculated by the method of Brackbill et al. [14] using the fluid densities at the interface and the droplet surface tension.

During the very initial time in the droplet impact on a rigid surface, a hammer pressure is generated due to the shock wave built up by the compression of droplet on the surface [15]. Trapaga and Szekely [16] have shown that the time scale of such compressible flow is at least an order of magnitude smaller than the overall impact and spreading process time typically found in a coating process. An incompressible flow assumption should yield reasonable results if the objective, in general, is toward studying coating formation by spreading of the droplet. Peak pressure (hammer pressure) during the compression period at early times, however, cannot be resolved [16]. The model has to include compressibility consideration in order to capture the hammer during droplet impact [17]. In this work, the model is incompressible, and hence we do not capture the hammer pressure in our simulations.

The initial conditions appropriate to the physical system shown in Fig. 1 are: at $t = 0$, $F = 1$ in the droplet shell, $F = 0$ in the droplet void; droplet velocity $U_0 = 5.25$ m/s, $T = T_0 = 325$ K; $u = v = F = 0$, everywhere else in the domain. It may be noted that the void in the hollow droplet is of the same gas (i.e., air) which surrounds the droplet. Boundary conditions for the problem considered are shown in Fig. 1.

3 Results and discussion

3.1 Impact process

The dynamic impact process of the hollow droplet on a flat surface is shown in Fig. 2. During the very initial times (0.05 ms, 0.075 ms) in the impact process when the droplet touches the surface we noticed entrapment of an air bubble. Such air bubble entrapment has also been studied experimentally and theoretically [18–20]. During the subsequent time in the impact process, the hollow droplet undergo deformation of the droplet shell and the void within the droplet (0.1 ms), stretching of the void cavity and thinning of the droplet shell (0.5 ms) followed by rupture of the shell (1.2 ms). At the *first stage* of the impact process, the lower hemispherical shell comes into contact with the substrate surface and progressively deforms. At the same time, the upper hemispherical shell proceeds with the motion with initial velocity. At the *second stage*, stretching of the void cavity and thinning of the droplet shell take place. At the *third stage*, rupture occurs at the periphery of the upper hemisphere. Between *first* and *third stages* a central counter jet forms which moves upward (0.5 ms). The flow of the droplet material in the centrally converging flow during the formation of the counter jet mixes with the entrapped air bubble, which formed during the very initial time in the impact process, and subsequently replaces it. In this way, the entrapped air bubble has no further effects on the droplet impact dynamics. The counter jetting phenomenon captured in our simulation is similar to that observed in the hollow droplet impact experiment reported in [8]. To the best of authors' knowledge, the experiment devoted to visualisation of the collision of a hollow liquid drop with a flat surface is reported only in [8]. The axisymmetric spreading along the surface takes place only in the initial period of time ($t \leq$ shell thickness$/U_0$). After this from the shell–surface contact location, which is away from the centre, a part of the liquid moves toward the centre generating a radial converging liquid stream. This creates the central counter jet (see Fig. 3). Liquid is continuously supplied to the counter jet from the shell, and the thickness of the shell continuously decreases which finally ruptures. Meanwhile, the radial converging flow in the central counter jet that is directed along the outer normal to the surface creates an upward movement of the counter jet. In order to further understand the cause of the formation of central counter jetting, the velocity and the pressure distributions in the droplet are shown in Fig. 3. We can see that during the impact process the flow from the upper hemispherical shell follows the spreading path (see Fig. 3a 0.3 ms). However, there is also a backward vortex

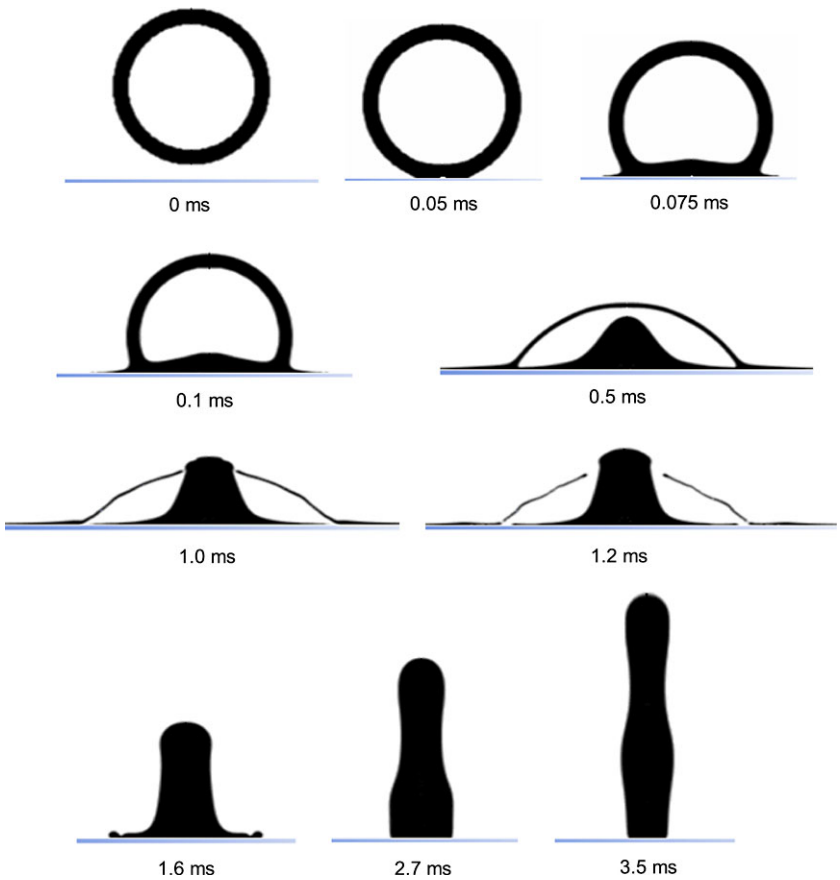

Fig. 2 Sequences of the hollow droplet impact on the surface. Impact conditions: outer diameter (D_0) 5.25 mm, void diameter (d) 4.389 mm (shell thickness = 0.4305 mm), impact velocity (U_0) of 5.94 m/s. During the very initial times (0.05 ms), entrapment of an air bubble at the centre of the impact point can be noticed

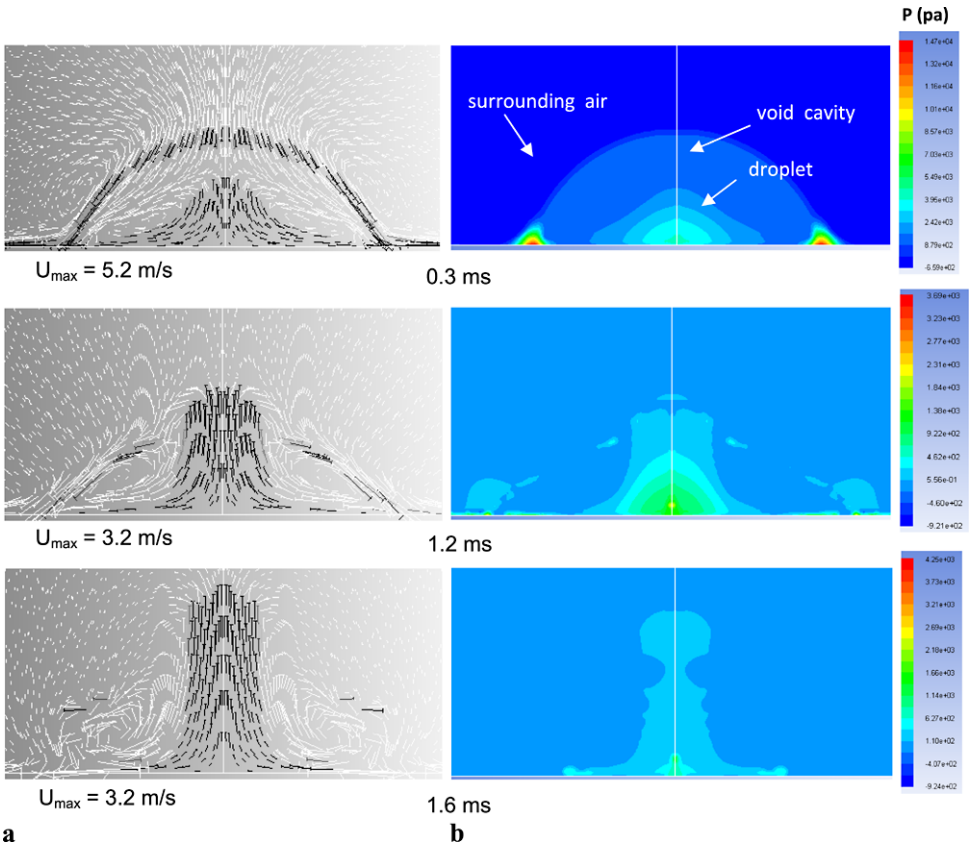

Fig. 3 (**a**) Velocity and (**b**) gauge pressure distribution in the hollow droplet at different time. The velocity vectors in white colour are in the air (surrounding and void cavity) and in black colour are in the droplet

from the shell–surface contact location, which is away from the centre, toward the centre of droplet. This backward flow is caused by a pressure build up at that location (see Fig. 3b at 0.3 ms). At subsequent time, the pressure build up location shifts towards the centre of the droplet (see Fig. 3b at 1.2 ms and 1.6 ms) and the backward vortex, generated earlier, creates an upward flow at the centre of the droplet.

3.2 Comparison with experiment

We observed earlier the formation of counter jetting during the impact of hollow droplet on the flat surface. Figures 4a and 4b show a comparison of the predicted droplet impact behaviour with the experimental result [8]. As can be seen, the predicted rupture of the droplet shell (1.0 ms) and the phenomenon of the counter jetting are very similar to those observed in the experiment. The length and mean thickness of the counter jet are also in good qualitative agreement with the experiment. The instantaneous length of the counter jet is quantitatively compared with experimental values in Fig. 4c, which shows that the predictions satisfactorily correspond to the experimental data.

3.3 Comparison with continuous dense droplet impact

It may be noted that the impact behaviour of a dense droplet is well studied, for example in [1–4]. The impact sequence of a continuous dense droplet is shown in Fig. 5a. The dense droplet is analogous to the hollow droplet, i.e., its mass is same as that of the hollow droplet. Therefore, the dense droplet will have the diameter of $0.746 \cdot D_0$ for having the same mass as that of the hollow droplet. The other impact conditions are same as that of the hollow droplet impact. After the impact, the dense droplet spreads radially along the substrate surface. A detailed discussion of this typical spreading behaviour for a dense droplet can be found in [1–4], and hence the discussion on this is not repeated here. This result is presented here in order to highlight the distinct feature of the hollow droplet impact. Comparing Fig. 5a with Fig. 2, the distinct impact behaviour of the hollow droplet can be noticed, specifically, the absence of the phenomenon of counter jetting during impact of the continuous droplet. In Fig. 5b, we compare the droplet spreading factor of the hollow droplet and an equivalent continuous droplet. The spreading factor is defined as the ratio of the instantaneous splat diameter to the initial droplet diameter. We find that for the hollow droplet the spreading factor is lower than the continuous droplet. Previously also, it was experimentally demonstrated that the dimensionless diameter of the ZrO_2 splat, under otherwise equivalent conditions, is significantly smaller for a hollow particle than for the dense one [7]. In the case of hollow droplet, much of the droplet

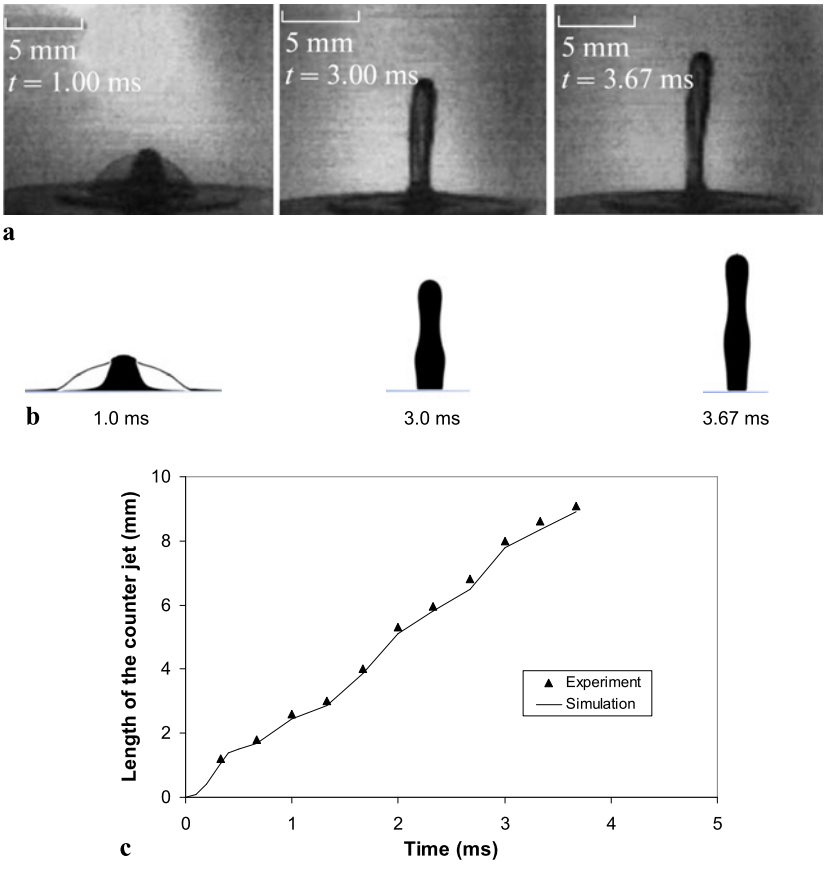

Fig. 4 Comparison of (**a**) the experimental [8] and (**b**) simulated hollow droplet impact behaviour on the surface. Impact conditions: outer diameter (D_0) 5.25 mm, void diameter (d) 4.389 mm (shell thickness = 0.4305 mm), impact velocity (U_0) of 5.94 m/s. The comparison is shown at the same scale; (**c**) time evolution of the counter jet length

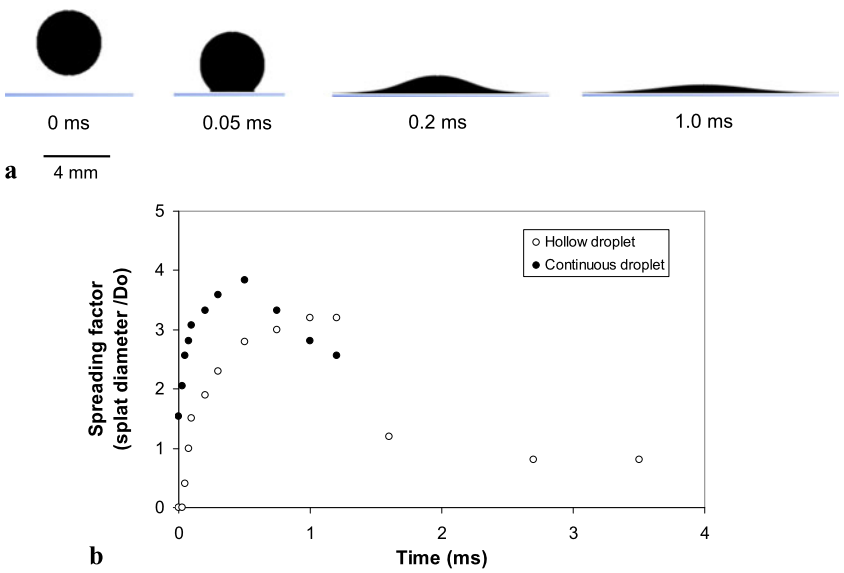

Fig. 5 (**a**) Sequences of the continuous dense droplet impact on the surface, (**b**) comparison of droplet spreading factor for hollow and equivalent continuous dense droplets

material goes into the counter jet, which causes a relatively slower spreading along the surface for the hollow droplet.

3.4 Influence of hollow droplet impact velocity

In order to study the influence of the droplet impact velocity on the impact behaviour, we performed simulations with two other impact velocities—one lower than the baseline impact velocity (i.e., 3 m/s) and the other higher than the baseline case (i.e., 20 m/s). The other impact conditions are kept same as the baseline case. Figure 6 shows the sequences of the droplet impact for these impact velocities. Comparing Figs. 6 and 2, it can be noticed that for these higher and lower impact velocities also the impact behaviour is quite

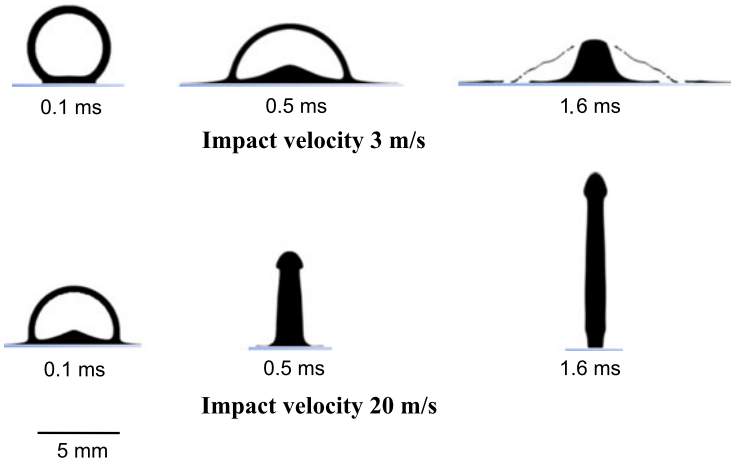

Fig. 6 Snapshots of the hollow droplet impact on the surface for different impact velocities

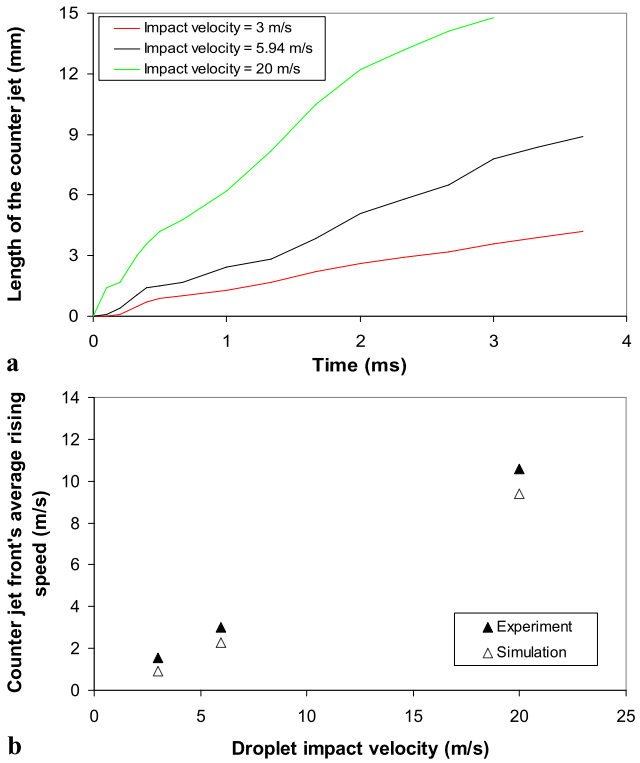

Fig. 7 (**a**) Time evolution of the counter jet length for different impact velocities, (**b**) comparison of the experimental [8] and simulated average rising speed of the counter jet front for different impact velocities

similar to that observed in the baseline case, notably the formation of counter jetting. However, the counter jet develops earlier, having higher length and lower mean thickness, for larger impact velocity. The mean thickness of the counter jet is 2.05 mm, 1.52 mm, and 0.92 mm for impact velocity of 3 m/s, 5.94 m/s, and 20 m/s, respectively. The rupture of the droplet shell is delayed when the impact velocity is low. In our simulations, the droplet shell ruptures at 1.6 ms, 1.2 ms, and 0.3 ms for impact velocity of 3 m/s, 5.94 m/s, and 20 m/s, respectively. Figure 7a shows the evolution of the counter jet length for different impact velocities. As noticed earlier, larger impact velocity causes earlier formation and faster growth of the counter jet having higher length. Figure 7b shows a comparison of the experimental and simulated results for the average upward rising speed of the counter jet front for different impact velocities. In the experiment, the mean speed of the counter jet is estimated from the instantaneous images of the droplet impact. In simulations it is estimated by averaging the different time velocity in the droplet near the front of the counter jet. For example, velocity field shown in Fig. 3a is used to estimate this. This may lead to some under prediction of the mean speed of the counter jet front, however, overall these predictions agree reasonably well with the experimental data.

3.5 Influence of hollow droplet shell thickness

In the baseline case, the shell thickness was 0.4305 mm. In order to study the sensitivity of the shell thickness, simulations with two other hollow droplet shell thickness of 0.75 mm and 1.0 mm are also performed. The other impact conditions are kept same as the baseline case. Figure 8a shows the sequences of the droplet impact for these cases. Comparing Figs. 8a and 2, it can be noticed that for these higher shell thickness also the impact behaviour is quite similar to that observed in the baseline case, notably the formation of counter jetting. The counter jet develops slightly earlier in a thicker shell because of more liquid flow from a thicker shell in the centrally converging flow, which was earlier shown as the cause of the formation of the counter jet. However, the rupture of the droplet shell occurs later in a thicker shell due to its more strength. In our simulations, the droplet shell ruptures at 1.2 ms, 1.3 ms, and 1.5 ms for droplet shell thickness of 0.4305 mm, 0.75 mm, and 1.0 mm, respectively. After rupture of the shell, growth of the counter jet is for all cases are quite similar, with slightly slower growth for a thicker shell (see Fig. 8b). The mean thickness of the counter jet is found to be more in a thicker shell (see

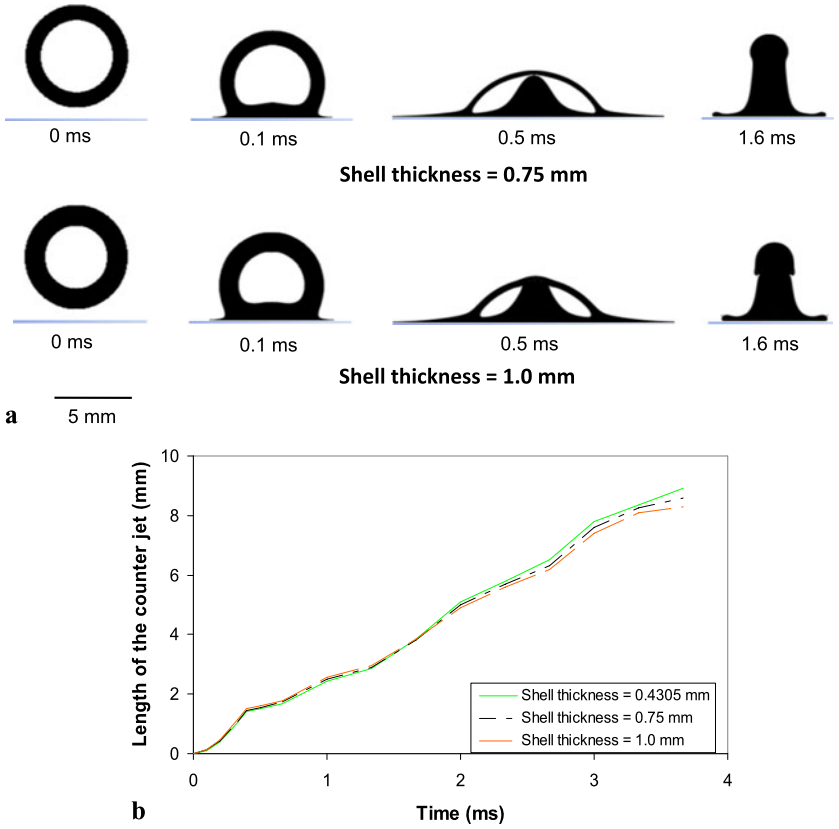

Fig. 8 (**a**) Snapshots of the droplet impact on the surface and (**b**) time evolution of the counter jet length for different shell thickness in the hollow droplet

Fig. 8a). The estimated mean thickness of the counter jet is 1.52 mm, 1.75 mm, and 1.95 mm for droplet shell thickness of 0.4305 mm, 0.75 mm, and 1.0 mm, respectively. Because of a thicker counter jet, its growth will be slower.

4 Conclusion

The results for impact of hollow droplet on a flat surface clearly show that the impingement process of hollow droplet has some new hydrodynamic features. The impact process of the hollow droplet undergoes deformation of the droplet and the void within the droplet, stretching of the void cavity and thinning of the droplet shell followed by rupture of the shell. A new phenomenon of central liquid counter jetting, also reported experimentally, is well captured. According to this, the liquid spreading is accompanied by the ejection of a central counter jet. The predicted length and mean thickness of the central counter jet, and the average rising speed of the counter jet front agree well with the experimental data [8]. The rupture of the droplet shell is delayed when the impact velocity is low. Larger impact velocity causes earlier formation and faster growth of the counter jet having higher length and lower thickness. Thicker shell in the hollow droplet results in earlier start of the formation of the counter jet, which subsequently has more thickness and lower length compared to a thinner droplet shell. The systematic understanding of the hydrodynamic behaviour of the hollow droplet impact developed in this work is a starting step to investigate the coating formed by hollow melt droplets [6]. In this regard, our future work will focus on including the solidification phase transition.

Acknowledgements The authors gratefully acknowledge the financial support from the EC FP7 Simuspray project (Grant No. 230715).

References

1. S.D. Aziz, S. Chandra, Int. J. Heat Mass Transf. **43**, 2841 (2000)
2. S. Kamnis, S. Gu, J. Phys. D, Appl. Phys. **38**, 3664 (2005)
3. S. Kamnis, S. Gu, T.J. Lu, C. Chen, J. Phys. D, Appl. Phys. **41**, 165303 (2008)
4. S. Chandra, P. Fauchais, J. Therm. Spray Technol. **18**, 148 (2009)
5. H. Tabbara, S. Gu, Appl. Phys. A, Mater. Sci. Process. **104**, 1011 (2011)
6. O.P. Solonenko, A.V. Smirnov, I.P. Gulyaev, in *5th International Workshop on Complex Systems*, Sendai, Japan, 2007, ed. by M. Tokuyama, I. Oppenheim, H. Nishiyama, vol. 982 (AIP Conference Proceedings, New York, 2008), p. 561
7. O.P. Solonenko, I.P. Gulyaev, A.V. Smirnov, Tech. Phys. Lett. **34**, 1050 (2008)
8. I.P. Gulyaev, O.P. Solonenko, P.Yu. Gulyaev, A.V. Smirnov, Tech. Phys. Lett. **35**, 885 (2009)
9. S. Kamnis, S. Gu, M. Vardavoulias, J. Therm. Spray Technol. **20**, 630 (2011)
10. J. Kovacik, J. Mater. Sci. Lett. **18**, 1007 (1999)

11. K. Shinoda, H. Murakami, J. Therm. Spray Technol. **19**, 602 (2010)
12. M.P. Planche, S. Costil, C. Verdy, C. Coddet, Appl. Phys. A, Mater. Sci. Process. **99**, 665 (2010)
13. Ansys Fluent 12.0 Theory Guide, Ansys, Inc., Canonsburg, PA 15317, USA, 2009
14. J.U. Brackbill, D.B. Kothe, C. Zemach, J. Comput. Phys. **100**, 335 (1992)
15. J.E. Field, Phys. Med. Biol. **36**, 1475 (1991)
16. G. Trapaga, J. Szekely, Metall. Mater. Trans., B Process Metall. Mater. Proc. Sci. **22**, 901 (1991)
17. R. Li, H. Ninokata, M. Mori, Prog. Nucl. Energy **53**, 881 (2011)
18. S. Chandra, C.T. Avedisian, Proc. R. Soc. Lond. Ser. A, Math. Phys. Sci. **432**, 13 (1991)
19. V. Mehdi-Nejad, J. Mostaghimi, S. Chandra, Phys. Fluids **15**, 173 (2003)
20. L. Chen, Z. Li, Phys. Rev. E **82**, 016308 (2010)